Nonlinear effects in transient electrothermal characterization of anatase TiO_2 nanowires

Xuhui Feng,[1] Xiaopeng Huang,[1] and Xinwei Wang[1,2,a)]
[1]*Department of Mechanical Engineering, 2010 Black Engineering Building, Iowa State University, Ames, Iowa 50011, USA*
[2]*School of Environmental and Municipal Engineering, Qingdao Technological University, People's Republic of China*

(Received 15 December 2011; accepted 23 March 2012; published online 16 April 2012)

As an effective transient thermal characterization technique, the transient electrothermal (TET) technique features a capability of measuring micro/nanoscale samples of diverse electrical conducting natures. In this work, single anatase titanium dioxide (TiO_2) nanowires fabricated using the electrospinning method are characterized using the TET technique. Time-dependent nonlinear effect is observed for both rise and fall stages in the voltage-time (*U-t*) response profile. The coated iridium film and soldered platinum pads possibly compromise the linear Ohmic effect and introduce undesired effects into the whole system. Two quantitative methods: generalized function analysis and direct capacitance derivation, are developed to suppress the nonlinear effect based on *U-t* profiles. Data processing is performed to determine the thermal diffusivity using global fitting under non-constant electrical heating. The effective thermal diffusivities from modified analysis processes stay in the range from 2 to 6 $\times$ 10^{-6} m^2/s. The results from both methods agree well with each other. The general function analysis method is also applicable for samples of short time thermal transport or for an experimental instrument that has relatively long rise time. © *2012 American Institute of Physics*. [http://dx.doi.org/10.1063/1.3702805]

I. INTRODUCTION

One-dimensional nanostructures, such as nanotubes and nanowires, have shown great potential in photoelectric and thermoelectric applications, especially in the micro/nanoelectronics industry.[1] Due to the significant scale reduction, the topics of thermal properties and transport inside such micro/nano-scale devices become increasingly crucial. A variety of techniques, such as the 3ω method,[2–5] flash method,[6–9] micro-bridge method,[10] and many others[11–16] have been developed for thermal transport and property characterization. Using electron beam and photolithography techniques, Kim *et al.*[17] fabricated a micro-scale suspended device to measure the thermal transport property of single multi-wall carbon nanotube (CNT) with known heat flow and temperature gradient at steady state. A similar technique using microfabricated devices[18] was employed to measure thermal and thermoelectric properties of one-dimensional nanostructures, including individual single crystalline silicon nanowires[19] and carbon nanofibers.[20] The thermal contacts between sample and microfabricated device were studied and platinum (Pt) deposition was applied to reduce the thermal contact resistance. Compared with steady-state methods, transient techniques present much reduced measurement times and are able to determine thermal diffusivity and specific heat simultaneously. Temperature-dependent thermal conductivity of skutterudite thin films was studied using a differential 3ω method in the cross-plane direction from 80 to 300 K.[3] Significant thermal conductivity reduction was observed compared with its bulk counterpart. For small-size samples such as single-wall[5] and multi-wall[4] CNTs, the 3ω method was also effective for measuring the thermal conductivity and thermal diffusivity. The flash method,[6] as a commonly used thermal measurement technique to measure disk-like materials, was advanced by Baba and Ono[7] by improving the uniformity of pulse heating and using a fast infrared radiation thermometer. Akoshima and Baba[8] applied the laser flash method to determine the thermal diffusivity of as-grown and solid super-growth single-wall CNT forest samples along the thickness direction. The pulsed-heating method was developed by Okuda and Ohkubo[21] to have successfully measured the thermal conductivity of thin dielectric films such as bulk fused quartz and silicon dioxide films down to a few hundred nanometers thick. The non-contact photothermal displacement technique[22,23] for measuring thermal diffusivity was used by detecting local transient surface displacement through photothermoelastic coupling of a pulsed laser beam. Further derivation based on heat-flow analysis provided the film conductivity and interface thermal resistance. Instead of focusing on surface motion, Wang *et al.*[24] measured the thermophysical properties of polymethyl methacrylate–Zirconium (IV) propoxide hybrid film by detecting the phase shift between the thermal radiation of the radiated sample surface and the modulated laser beam.

Transient techniques that include laser beam or electrical heating, such as transient electrothermal (TET) technique,[25,26] optical heating and electrical thermal sensing (OHETS) technique,[27] transient photo-electrothermal

a)Author to whom correspondence should be addressed. Electronic mail: xwang3@iastate.edu. Tel.: 515-294-2085. Fax: 515-294-3261.

technique,[28] and pulse laser-assisted thermal relaxation technique[29] have been broadly utilized in our group for measuring thermophysical properties of micro/nano film/wire/tubes. As one of these transient thermal characterization techniques, the TET technique has demonstrated great advantages from several perspectives. First, the TET technique can be applied to metallic, nonconductive, and semi-conductive one-dimensional small-scale structures including films, wires, and tubes. Second, the TET technique features much stronger signal levels (hundreds to thousands of times higher) compared with the 3ω and OHETS techniques. Third, the TET technique requires much reduced response time (usually less than 1 s). These advantages of TET have been proven in determining the thermal diffusivity of different kinds of small-scale materials, such as Pt wire,[25] organic poly(3-hexylthiphene) film,[30] and anatase titanium dioxide (TiO_2) thin film.[26] To utilize the TET technique, linear voltage-current response (Ohmic effect) is required to calculate variation of resistance and generated electrical heating during the process. For semi-conductive and non-conductive samples, a metallic coating is required to ensure that the sample has metallic-like characteristics and meanwhile the resistance is confined within a proper range.

For small-scale materials whose dimensions fall into the nanometer range and whose surface is coated with a metallic layer, great care should be exercised during sample preparation to minimize unnecessary effects such as thermal contact resistance, capacitance effect, inductance effect, and so on. These effects bring unpredictable influences to the utilization of the TET method and also uncertainty to the analysis of experimental data. The voltage-time (U-t) response of some samples presents obvious deviation from regular U-t curve of TET technique and also induces difficulty for determining an appropriate starting point for data processing. The same situation would happen when the current source with a long rise time is applied to materials that have relatively short thermal transport times. Therefore, modified data analysis is required to suppress these effects and to acquire more accurate thermal response of the sample. In Sec. II of this work, experimental principle and theoretical background of the TET technique is introduced, along with TET profiles of various samples showing differences between standard and deviated U-t curves. In Sec. III, the sample preparation procedure of single anatase TiO_2 nanowire is introduced to give a possible reason why deviations are generated. Two quantitative models are developed to process the experimental results. Modified profiles and results are presented and analyzed to demonstrate the validity of these models.

II. EXPERIMENTAL METHOD

A. Experimental configuration

In the TET technique, the to-be-measured sample is suspended between two metal (copper, aluminum, etc.) electrodes and both ends of the sample are pasted to the electrodes using conductive paint to enhance electrical conduction and to reduce thermal contact resistance. This

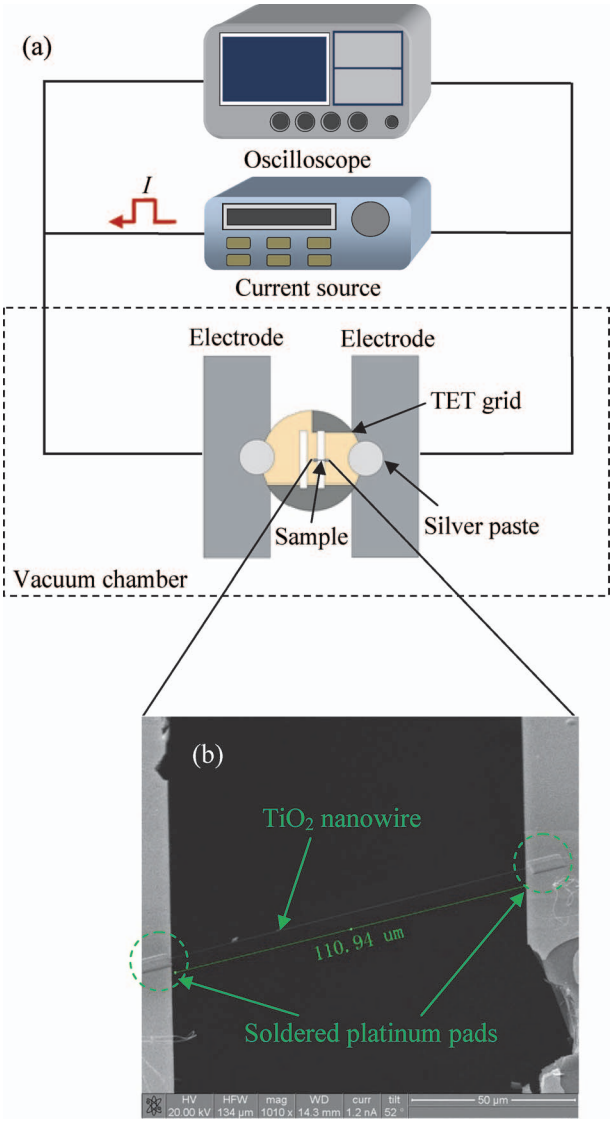

FIG. 1. (a) Experiment configuration of the TET technique and (b) SEM picture of the soldered nanowire.

configuration is clearly seen in Fig. 1(a) except that in this figure, the sample is a round-shaped TEM grid with the nanowire suspended over one slot. Generally, samples are simply suspended on electrodes without further processing. Bases with a suspended sample similar to the one shown in Fig. 1(a) are then positioned in a vacuum chamber ($<1.0 \times 10^{-3}$ Torr) as illustrated by the dotted line in Fig. 1(a) to minimize the air convection effect. A current source (Keithley 6221 dc and ac current source) is connected to the base to provide a constant current signal. The rise time of the device is negligible compared with the thermal response time of the sample. A high-speed oscilloscope (Tektronix TDS 7054 digital phosphor oscilloscope) with 1 MΩ impedance is employed to record the transient U-t response. All connections and cables in the experimental setup are shielded to suppress environmental noise. At the beginning of the experiment, a dc current is provided through the sample to introduce electrical heating. The induced temperature evolution of the wire strongly depends on the heat transfer along it and the

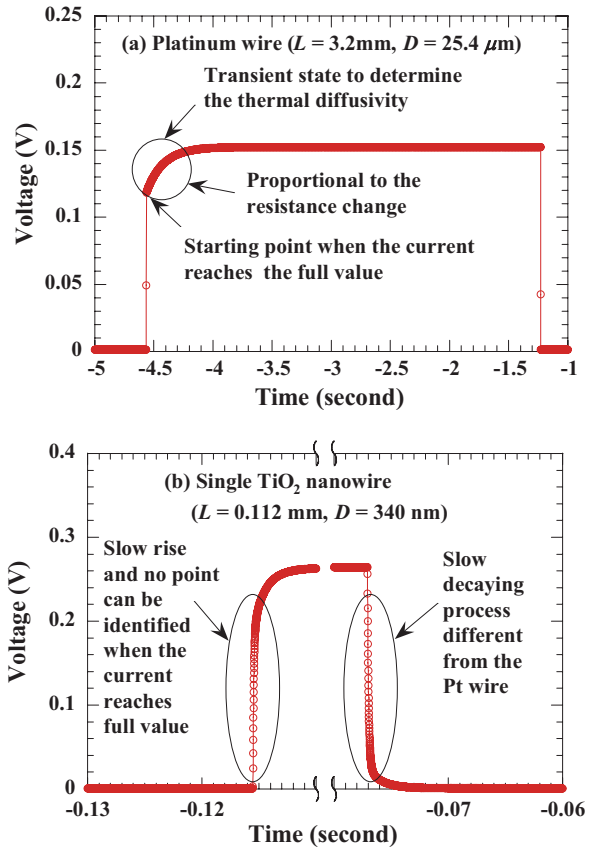

FIG. 2. (a) Original *U-t* profile for platinum wire, the diameter of which is 25.4 μm and (b) original *U-t* profile for single anatase TiO_2 nanowire, the diameter of which is 340 nm, containing both rise and fall stages.

consequent temperature rise leads to resistance change, which is converted to the voltage change recorded by the oscilloscope. A typical *U-t* profile of platinum (Pt) wire is presented in Fig. 2(a). It is observed in this plot that the voltage is zero before the current is provided and then immediately rises to an anticipated non-zero value as soon as the current feeding starts. Under continuous constant current, the voltage recording on the oscilloscope increases and then reaches a stable value if the cycle time is long enough. Particularly, for the rise state, only very few irrelevant points emerge before reaching the anticipated voltage, indicating that the voltage response is linear and there is no substantial impact to reduce the current passing through the Pt wire. At the moment when the current feeding is terminated, the voltage instantaneously decreases to zero with very few intermediate points, implying again that only the resistance of the Pt wire takes effect in the measurement.

B. Theoretical principles

In order to obtain the thermal diffusivity from a *U-t* profile as shown in Fig. 2(a), a theoretical solution is required for data fitting. The experimental setup can be interpreted as a one-dimensional heat transfer problem as shown in Fig. 1(a) and the governing equation is

$$\frac{\partial(\rho c_p T)}{\partial t} = k\frac{\partial^2 T}{\partial x^2} + q_0, \tag{1}$$

where ρ, c_p, and k are density, specific heat, and thermal conductivity of the sample, respectively. A constant temperature boundary condition is applied considering the fact that the metal electrodes are much larger than the dimension of the sample and heat dissipates quickly. Details for solving this equation are given in our previous work.[25] x is the sample's axial direction. Only the analytical solution is presented here for discussion purpose. By integrating the solution $T(x, t)$ over the whole length, the average temperature of sample $T(t)$ is calculated as

$$T(t) = \frac{1}{L}\int_{x=0}^{L} T(x,t)\,dx = T_0 + \frac{8q_0L^2}{k\pi^4}\sum_{m=1}^{\infty}\frac{1-exp[-(2m-1)^2\pi^2\alpha t/L^2]}{(2m-1)^4}. \tag{2}$$

Given enough thermal transport time, the temperature distribution along the sample reaches a steady state and equals $T_0 + q_0L^2/(12k)$ based on Eq. (2). q_0 is the electrical heating power per unit volume and is expressed as $q_0 = I^2R/(AL)$, in which A and L are the cross-sectional area and length of the sample, respectively. Normally, in solving this governing equation, heating power is assumed constant. This can be done by carefully controlling the heating current to make sure the sample temperature rise is moderate. Normalization of average temperature increase into dimensionless form yields

$$T^* = \frac{96}{\pi^4}\sum_{m=1}^{\infty}\frac{1-\exp[-(2m-1)^2\pi^2\alpha t/L^2]}{(2m-1)^4}. \tag{3}$$

The voltage evolution (U_{sample}) recorded by the oscilloscope is directly related to the average temperature change of the sample as

$$U_{sample} = IR_0 + I\eta\frac{8q_0L^2}{k\pi^4}\times\sum_{m=1}^{\infty}\frac{1-\exp[-(2m-1)^2\pi^2\alpha t/L^2]}{(2m-1)^4}, \tag{4}$$

where U_{sample} is the voltage over the sample recorded by the oscilloscope, I is the constant current through the sample, R_0 is the sample resistance without heating, and η is the temperature coefficient of resistance of the sample. Therefore, it is obvious that the measured voltage change is inherently proportional to the temperature evolution of the sample. In order to obtain the thermal diffusivity, global fitting of the experimental data using a theoretical solution is performed by trying different trial values of thermal diffusivity and the best fit (least square method) gives the thermal property of the sample.

C. Linear and nonlinear response

An important step in the global fitting procedure is to locate the starting point at which the resistance of the sample can be evaluated. If there is no other effect to shunt the current, the voltage should develop like the one in Fig. 2(a) and can be used to represent the resistance-time profile. As

indicated in Fig. 2(a), at the starting point, the current through the sample already reaches the full value, and Ohm's law can be used to describe the relation between the measured voltage and the current through the sample. However, after detailed comparison between the original *U-t* profiles of Pt wire and single TiO_2 nanowire [Fig. 2(b)], it is obvious that significant dissimilarity exists. For a Pt wire, at the moment the current is provided, the voltage increases immediately to the value that contains full current and resistance, with simply one abrupt increasing point due to the finite rise time of the current source. Additionally, the decaying state caused by termination of the current is also instantaneous and contains no irregular points. For a single TiO_2 nanowire, as seen in the time range from −0.13 to −0.11 s in Fig. 2(b), when a current is provided, the voltage increases gradually and there is no distinct starting point when the current through the sample reaches its full value. Therefore, the voltage-time profile cannot be used directly to represent the resistance-time profile and to evaluate the thermal transport. In fact, the observed *U-t* profile contains conjugated information about the nonlinear response of the system and thermal transport in the nanowire. This abnormality suggests that the total current from the current source does not entirely flow through the nanowire until a certain moment. Other effects shunt the current so the current fed through the nanowire increases with time slowly before it reaches its full value. In the range from −0.08 to −0.06 seconds in Fig. 2(b), it is the decaying state which more distinctly shows the presence of unknown effects because during this stage, when the current feeding stops the voltage does not drop to zero immediately. Instead it exhibits a discharge-like effect, showing that there may be other current sources in the circuit. This is possibly attributed to some capacitance effects generated from a capacitor-like slot structure on the TEM grid as discussed later.

III. DATA ANALYSIS AND RESULTS

A. Sample preparation

From the previous discussion, the nonlinear time-dependent effect appears for particular samples and is speculated to be substantially related to sample preparation. The characterized sample in Fig. 2(b) is a single anatase TiO_2 nanowire fabricated via the electrospinning technique in our laboratory. During sample fabrication, 1.5 g titanium tetraisopropoxide [$Ti(OiPr)_4$, from Aldrich] was mixed with 3 ml ethanol and 3 ml acetic acid in a beaker. After 10 min the mixture was combined with 7.5 ml ethanol that contained 4.5 g of poly(vinyl pyrrolidone) (PVP, Aldrich, Mw ≈ 1 300 000), followed by magnetic stirring in a capped vial. The well-stirred solution was then immediately transferred into a syringe equipped with a 23-gauge stainless-steel needle. The needle was connected to an ultra-high voltage source that can provide about 20 kV voltage. A specially pre-processed TEM grid [Fig. 1(a)] was used as the collector and was positioned about 8–10 cm below the needle. This TEM grid was made of single-sided polished silicon and has two through slots of 1.5 mm × 0.1 mm. The TEM grid surface was partially coated with a thin gold film to ensure one slot was nonconductive to serve as separate electrodes as introduced in the TET technique principle section. The two parallel sides of the selected slot act to create symmetric electrical forces and to collect highly oriented nanowires. With the ultra-high electric field of about 2 kV/cm, the polymer solution was ejected from the needle tip and stretched into continuous ultrathin nanowires onto the TET grid. The diameter and concentration of the nanowires are controllable by adjusting the concentration of PVP content, the voltage and the distance between the needle and collector.

As-spun nanowires were left in open air for ∼5 h to allow for complete hydrolysis of $Ti(OiPr)_4$. Then the nanowires were annealed at 500 °C to achieve crystalline transition from amorphous to anatase and also to help with degradation of PVP content. After selectively removing other nanowires by tweezers, only one TiO_2 nanowire was left suspended over the slot. Then the remaining anatase TiO_2 nanowire was coated (Q150T sputter coater) with a 15-nm thick iridium film to make the sample conductive for thermal characterization. In order to reduce thermal contact resistance and enhance electrical conduction, a focused ion beam-assisted platinum soldering process (Quanta 3D Dual-beam system) was used to deposit thin Pt pads (10 μm × 6 μm) on both ends of the nanowire. A scanning electron microscopy (SEM) image of a prepared Ir-coated and Pt-soldered single TiO_2 nanowire is shown in Fig. 1(b). The length of this TiO_2 nanowire is 110.94 μm and the diameter is 340 nm. After completing required processing, this sample is ready to be placed in a vacuum chamber for thermal characterization using the TET technique. By operating the TET procedure, original *U-t* profiles are recorded using the oscilloscope. However, as discussed before, the *U-t* profile of the single TiO_2 nanowire contains more than just the effect of resistance and the possible reason is because the treatments such as coating on the TEM grid and soldering probably have induced a capacitance effect in the whole circuit. This effect has brought nonlinear effects to the current flow and the consequent voltage evolution of the sample. Due to the complicated nature of sample preparation, two quantitative models and related data analysis are presented in following sections to rule out the nonlinear time-dependent effect.

B. Nonlinear effect analysis

1. Generalized function analysis

In order to exclude undesired effects and to acquire pure linear response, a simplified physical model is presented in Fig. 4(a). The whole experiment setup is generalized into a circuit in which the nanowire itself is represented by an equivalent resistor R_0 and other effects together exhibit as another parallel element (e.g., capacitor). Based on Fig. 2(b), the current passing through the nanowire follows a relation $I_0 f_1(t)$, here $f_1(t)$ is a general form of a time-relevant function. For example, if the capacitance effect is taken into consideration, $f_1(t)$ can be expressed as $[1 - \exp(-t/RC)]$. After detailed examination, the voltage change with time of the nanowire does not exactly fit a capacitor charging process. A possible reason is that the resistance R in the time constant RC

is affected by other effects (heating effect in R_0) which causes time-dependent characteristics. Therefore, a generalized function analysis is exercised to exclude the unnecessary nonlinear effects by universally expressing the current as $I_0 f_1(t)$, regardless of the particular form of the nonlinear effect. Due to the heating effect introduced by the current, the resistance of the sample will change and is expressed as $R_0[1 + f_2(Q)]$, in which Q is the non-constant electrical heating proportional to square of the current passing through the nanowire, I^2. To the end, the voltage over the whole nanowire obeys Ohm's law as

$$U = I_0 f_1(t) R_0[1 + f_2(I^2)]. \quad (5)$$

If two different currents I_{01} and I_{02} are considered, the ratio of the induced voltages is

$$\frac{U_1}{U_2} = \frac{I_{01} f_1(t) R_0\left[1 + f_2\left(I_1^2\right)\right]}{I_{02} f_1(t) R_0\left[1 + f_2\left(I_2^2\right)\right]}. \quad (6)$$

Here the non-constant heating source is known to be included within the f_2 term. During the TET measurement, the resistance change induced by electrical heating is relatively small compared with the initial resistance. Because the generated electrical heat is linearly dependent on the square of current passing through the nanowire: $I^2 = I_0^2 f_1^2$, Eq. (6) can be simplified while ignoring the high-order terms as

$$\frac{U_1}{U_2} = \frac{I_{01}}{I_{02}}\left[1 + f_2\left(I_1^2 - I_2^2\right)\right], \quad (7)$$

in which only one term is left other than the ratio of currents. If there is no electrical heating effect, $[f_2({I_1}^2 - {I_2}^2)]$ should be zero and only the ratio of currents remains. Typically, the resistance of the sample changes because of the temperature change induced by electrical heating. In Eq. (5), the $f_1(t)$ emerges as the nonlinear factor and influences the current distribution in the whole experimental system. By applying this method to obtain Eq. (7), this nonlinear factor is constrained into a term much smaller than 1. Therefore, the ratio of voltages mostly contains impacts from heat transfer along the nanowire. For a particular TiO_2 nanowire (sample 6), two currents 6 μA and 14 μA are used and the ratio is presumed as a constant value 2.33 if no electrical heating and other effects are considered. Nevertheless, from Fig. 3, the ratio curve based on signals of both currents is presented. It is seen that the ratio increases very quickly from about 0.6 and then stabilizes around 2.5, implying that there could be another effect creating a time-dependent impact on the current distributed to the nanowire and this affects only a very small portion of the data. This proves again that the assumption to rule out small amounting terms is reasonable. This ratio curve is also plotted out to be compared with the plot in Fig. 2(a). It is apparent that after this processing, the ratio plot features more metal-like characteristics similar to the voltage response of Pt wire. The number of irregular points before achieving the anticipated value is also significantly less than the original U-t profile of single anatase TiO_2 nanowire. It proves that the nonlinear effect in current evolution has been suppressed significantly as seen in Eq. (7) so that less irrelevant points are observed. Further data processing to eliminate the first several irregular points will be discussed later.

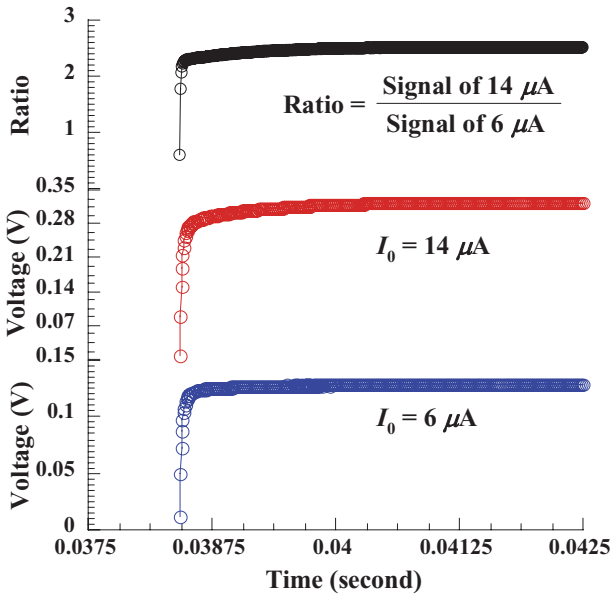

FIG. 3. Original U-t profiles of two different currents: 14 μA and 6 μA and the derived ratio profile based on two voltage profiles for sample 6.

2. Direct derivation of capacitance effect and resistance profile

As discussed before, from Fig. 2(b), both the rise and fall states are observed to be very similar to capacitor charging and discharging behaviors. Although it has been examined that these two profiles do not exactly follow the exponential relation of typical capacitors, this is likely because the time constant does not stay constant due to impact from other effects (heating in the nanowire) on the capacitors. A method is developed in this section to calculate the capacitance that appears in this RC circuit [Fig. 4(a)] based on U-t profiles. A simple assumption is made that in this circuit, only the nanowire and another capacitor are connected in parallel to form a resistance-capacitance circuit and no other elements or effects are considered, as shown in Fig. 4(a). Therefore, the overall current passing through the capacitor and nanowire will always be constant I_0. After the current through the capacitor is obtained, the current passing through the nanowire is deduced accordingly and so is the resistance change of the nanowire. With an actual resistance-time (R-t) profile, the global fitting is adopted again for determining the thermal diffusivity.

According to the definition, capacitance C is relevant to the voltage between two parallel plates U and also the amount the charge stored q as $q = C \times U$. Based on the working principle of the charging process of a capacitor, with the increase of voltage drop generated from the accumulated charges the charging current gradually decreases with time. The current that charges the capacitor is expressed as $I_{charging} = C \times (dU/dt)$. In addition, without considering heating effects at the first few moments, the resistance of the nanowire can be treated as a constant R_0 and the current I passing the nanowire then follows the form U/R_0. The summation of these two portions constitutes the overall current I_0 from the current source,

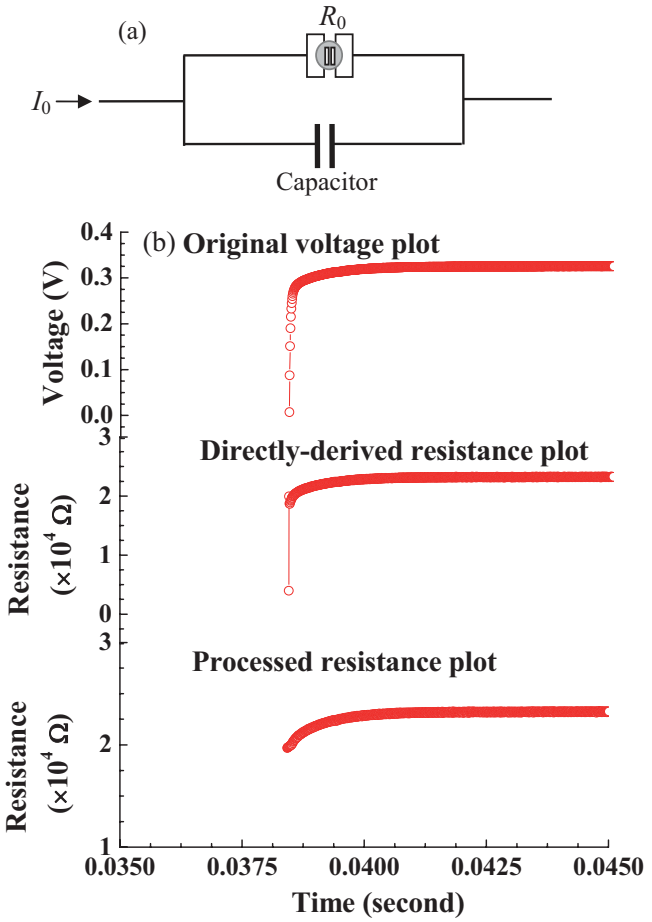

FIG. 4. (a) Simplified RC circuit model to describe the nonlinear effect and (b) original *U-t* profile, derived *R-t* profile from the direct derivation method and the further processed *R-t* profile with modified starting points. The data are for sample 6.

as expressed in Eq. (8),

$$C\frac{dU}{dt} + \frac{U}{R_0} = I_0. \tag{8}$$

Due to the high resolution of the oscilloscope, the first three or four data points of the voltage-time profile are applied reasonably because within such a limited increasing range, the heating effect is negligible and the resistance is then assumed constant. The solution to Eq. (8) is obtained as

$$U = I_0 R_0 \left[1 - \exp\left(-\frac{t}{R_0 C}\right)\right], \tag{9}$$

with the measured values of U and t, it is not hard to use exponential fittings to determine the coefficient I_0R_0 and R_0C, and then obtain the capacitance C and initial resistance R_0. When voltage rises later on, the overall relation reflected by Eq. (8) is still applicable except that the resistance R does not remain constant any more. The resistance is consequently calculated further based on Eq. (8) with the data from *U-t* profile,

$$R(t) = \frac{U}{I_0 - CdU/dt}. \tag{10}$$

Equation (10) gives the intrinsic nanowire resistance development with time by directly deriving the nonlinear capacitance effect based on the *U-t* profile. In order to confirm the validity of the RC circuit assumption, we calculate the capacitance of the same sample (sample 6) at different currents and different processes. With the *U-t* data from current 14 μA, the capacitances calculated from charging and discharging processes are 1.18 nF and 1.07 nF, respectively. Based on the voltage data under current 6 μA, the capacitance for the charging process is 1.02 nF. These capacitances from different currents and processes are very consistent which proves the rationality of the RC circuit assumption. For the same sample (sample 6) applied in the generalized analysis section, its original *U-t* profile from the oscilloscope and *R-t* profile from the above derivation method is presented in Fig. 4(b). In Fig. 4(b), the top plot is the original *U-t* profile of a gradual increasing trend of voltage and it is impossible to use the *U-t* profile to obtain the resistance change. After utilizing the data analysis based on Eq. (10), the obtained resistance curve in the middle curve in Fig. 4(b) presents significantly improved development characteristics. This curve is very similar to the *U-t* profile of the platinum wire shown in Fig. 2(a) and is much more ideal for global fitting to determine the thermal diffusivity. Compared with the ratio profile from the generalized analysis, the resistance curve contains less irrelevant points in the rise state and demonstrates a more distinct starting point to evaluate the resistance change of the nanowire.

However, it is further observed in the middle curve in Fig. 4(b) that with a significantly improved resistance profile, a few abnormal points still exist, with the resistance value about 4000 and 20 000 Ω. These irregular points are probably affected by conjugated electrical heating, thermal transport and some other unknown effects. Although the heating effect is relatively small at the beginning, the point at 4000 Ω cannot be ignored and is instead used to explore the actual value under normal heating conditions. To further process the data for better analysis, a strategy is developed by considering the linear relation between resistance variation and heating power, which is related to the square of voltage U^2. Therefore, for any initial resistance R_0, its real value is determined as

$$R_0 = R_1 - \frac{\int_{t_0}^{t_1} U^2 dt}{\int_{t_2}^{t_3} U^2 dt}(R_3 - R_2), \tag{11}$$

in which R_1, R_2, R_3 are all known resistance values of particular points selected from the normal range when voltage rises. By using the relationship between heating power and resistance increase, the value of irregular points are further explored and the corrected resistance profile is displayed in the bottom plot in Fig. 4(b). Comparison between the middle curve and bottom curve in Fig. 4(b) explicitly demonstrates that after the processing using Eq. (11), the irregular points are eliminated. The resistance increases from a reasonable value and then follows a typical evolutionary tendency considering heating effect and thermal transport. This profile is the one that is directly fitted with the theoretical temperature profile to acquire the thermal diffusivity. The same process is also used to correct the irregular points presented in Fig. 3.

C. Data processing

Based on the above methods and derived equations, further data processing can be performed to obtain the thermal diffusivity. For the sample in Fig. 3, two profiles of 6 μA and 14 μA currents are used for the ratio-time profile. The ratio of signals from two different currents will attenuate unnecessary effects and mostly contain effects from heating and thermal transport, as shown also in Fig. 3. This ratio profile is then normalized into a dimensionless form for fitting purposes. For theoretical calculation, from Eq. (1), the heat source does not stay constant because the current passing through the nanowire is a varying value during the experiment. Hence, numerical simulation is employed in this work to provide theoretical data with consideration of a non-constant heat source as $U^2(t)/R$. A one-dimensional scheme is employed to create the computing mesh and the governing equation [Eq. (1)] is discretized along both time and spatial dimensions. The average temperature of the whole nanowire is calculated at every time step and the temperature evolution with time is thus obtained. By normalizing the temperature variation and using different thermal diffusivity values, the best fitting is identified when the error between the simulated normalized temperature profile and the experimental normalized ratio profile reaches the minimal level (least square method) and this value is determined as the effective thermal diffusivity of the nanowire. A comparison figure based on the generalized analysis method is displayed in Fig. 5. Based on the fitting, the effective thermal diffusivity of this sample is determined as 2.44×10^{-6} m^2/s. Combined with the calibration process discussed in our other work,[26] the thermal conductivity and density of the single TiO_2 nanowire can be determined. This method for data analysis provides a novel perspective to suppress particular forms of nonlinear effects and to maintain the linearity characteristic in experimental data, as shown in Eq. (7). Instead of processing a single *U-t* profile, the ratio that has inherited linearity of current is more appropriate for data processing. Not only the nonlinear effects are minimized, but the impacts from a long rise time of the current source can also be suppressed using data from different currents. Similarly, thermal characterization of materials with ultra-short thermal transport time can be carried out using this method. For uncertainty analysis purposes, the thermal diffusivity is altered and related numerical fitting curves are shown to indicate that the uncertainty of this data processing is around 7%.

Applying the further processed resistance profile in Fig. 4(b) for global fitting, a fitted profile is shown in Fig. 6 and the determined thermal diffusivity is 2.30×10^{-6} m^2/s, while the two fittings show the uncertainty of global fitting is about 8%. This thermal diffusivity agrees well with the value determined, based on generalized analysis which was 2.44×10^{-6} m^2/s, with about 6% difference. This difference arises because of several reasons. First, during the implementation of the global fitting technique, theoretical values are calculated using the numerical simulation method as introduced in the last paragraph. However, in the generalized analysis, the heat power is expressed as $U^2(t)/R$, in which the resistance is a constant since its variation details remain unknown. In the direct derivation method, the resistance change is directly deduced under and is consequently used to calculate the heating power as $U^2(t)/R(t)$. Second, in generalized analysis, derivation of ratio data requires two sets of experimental data but only one set of data is used for fitting purpose. Selection of experimental data from different currents could introduce differences in the thermal diffusivity to a certain degree. Detailed observation and comparison between Figs. 5 and 6 show that within the time range from 0 to 4 ms, experimental results obey mainly similar trends, results from the direct derivation method present more fluctuations and results from the generalized analysis give a smoother feature. This distinction is also supported by the analytic expression of both methods, as shown by Eqs. (7) and (10). For the generalized analysis, it is clearly seen in Eq. (7) that the ratio is majorly dependent on the current I_{01} and I_{02}, and the nonlinear effect is only a very small portion, much less than 1. For example, this nonlinear function takes only 7% when using general analysis to acquire the ratio curve. For the direct derivation method, the nonlinear capacitance effect is fully contained to obtain the pure resistance change and thus the fluctuation contained in the data transfers into the expression of resistance. Also

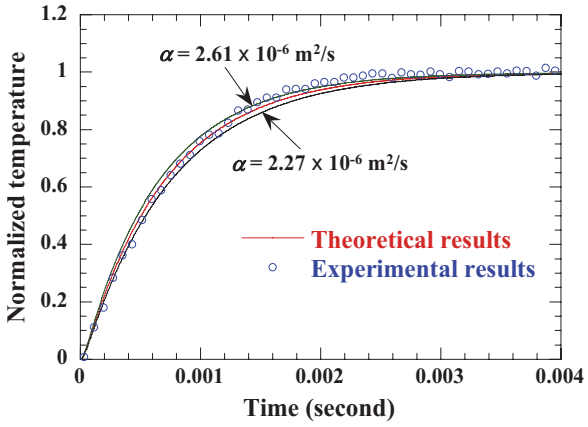

FIG. 5. Comparison plot of theoretical results and experimental data using the generalized analysis method for sample 6, along with other two theoretical curves to show the uncertainty of this data fitting process.

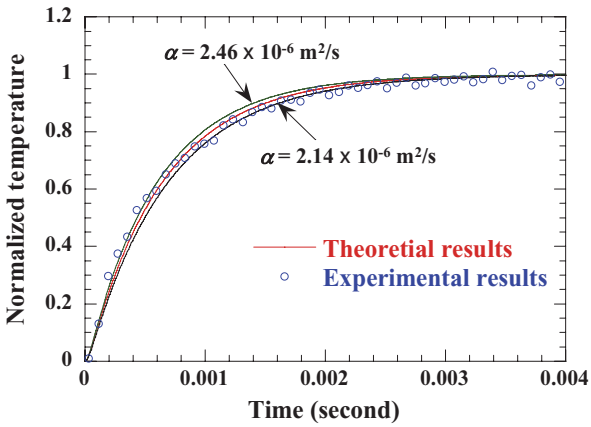

FIG. 6. Comparison plot of theoretical results and experimental data using the direct derivation method for sample 6, along with two other theoretical curves to show the uncertainty of this data fitting process.

TABLE I. Corresponding results calculated from generalized analysis and direct derivation methods for eight nanowire samples.

Sample	$\alpha_{1,eff}$[a] ($\times 10^{-6}$ m^2/s)	$\alpha_{2,eff}$[b] ($\times 10^{-6}$ m^2/s)	k_{eff}[c] (W/m · K)	$\alpha_{1,real}$[d] ($\times 10^{-6}$ m^2/s)	$\alpha_{2,real}$[e] ($\times 10^{-6}$ m^2/s)
1	2.94	3.27	4.17	1.30	1.45
2	2.69	2.61	2.26	1.92	1.75
3	4.94	6.62	7.25	4.18	5.61
4	5.91	5.61	6.72	4.60	4.37
5	2.01	2.01	2.42	1.51	1.40
6	2.44	2.30	4.14	2.14	2.02
7	2.14	1.71	4.09	1.65	1.19
8	2.40	2.03	5.85	1.45	1.16

[a]$\alpha_{1,eff}$: the effective thermal diffusivity obtained based on the general function analysis method.
[b]$\alpha_{2,eff}$: the effective thermal diffusivity obtained based on the direct derivation method.
[c]k_{eff}: the effective thermal conductivity.
[d]$\alpha_{1,real}$: the real thermal diffusivity obtained based on the general function analysis method.
[e]$\alpha_{2,real}$: the real thermal diffusivity obtained based on the direct derivation method.

in the direct derivation method, determination of the capacitance C is only based on a few points at the beginning of the process.

Both the generalized analysis and direct derivation prove to be feasible methods to rule out the nonlinear effect and to acquire pure resistance or voltage data for global fitting, as shown in Figs. 3 and 4(b). Table I lists the thermal diffusivities of all eight nanowire samples using the two methods and graphic comparison between two sets of thermal diffusivity is displayed in Fig. 7. The thermal diffusivities calculated by using both methods fall mainly in the range from about 2 to 6.5 $\times$ 10^{-6} m^2/s with similar distribution and only very few discrepancies, suggesting that both methods are capable of excluding nonlinear effects to give more accurate thermal diffusivity. Detailed percentages of differences between the two sets of thermal diffusivity calculated from the two methods are mostly lower than 15%, except sample 3 and sample 7, the differences of which are about 25%. Considering the consistent vicinity of other data, the distinct deviations for samples 3 and 7 may be attributed to particular disturbances in the preparation procedure. Except for these two value sets, other data demonstrates high agreement. Further examination

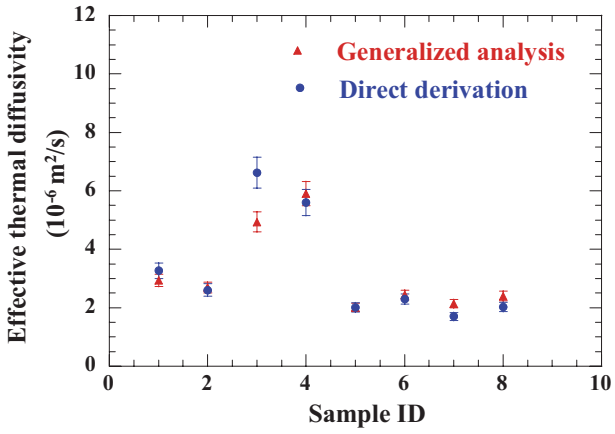

FIG. 7. Effective thermal diffusivities calculated from the two methods for all nanowire samples.

reveals that the thermal diffusivities from direct derivation are a little lower than those from generalized analysis while exceptions are identified for samples 1 and 3. As analyzed before this difference is caused by several factors, such as different consideration of heat sources, different selection of experimental data and different simplifications made to derive the capacitance. In addition, distinct basis of the two methods is also accountable. For generalized analysis, due to the unknown factors of nonlinear effects, an expression from Ohm's law is applied by simplifying those effects into a general function form f_1 regardless of any particular effects. For direct derivation, assumptions are made that the whole setup is a simple RC circuit and at the very beginning the electrical heating effect is negligible, thus the resistance is treated as a constant. Under these circumstances, direct derivation presents higher quantitative accuracy although its utilization requires more strictly examined conditions. On the other hand, the generalized analysis presents higher adaptability to a variety of conditions. For instance, because it is much less concerned with the time-related effects, it can be used to handle samples with faster thermal response times or current sources with relatively long rise times.

The thermal diffusivity obtained so far is an effective value, meaning that the impact from the iridium coating is still included. Based on the nature of the coating, the overall effective thermal diffusivity is a superposition of the thermal diffusivity of both titania nanowire and iridium film. The Wiedemann-Franz law can be applied to interpret the influence of iridium coating because its thermal and electrical properties are closely related. With the effective thermal conductivity (k_{eff}),[26] the overall effective volume-based specific heat of the nanowire is obtained as $C_{eff} = \rho c_p = k_{eff}/\alpha_{eff}$. Then the real thermal diffusivity is calculated as $\alpha_{real} = \alpha_{eff} - (L_{\text{Lorenz}} TL/RA_w C_{eff})$, in which L and A_w are length and cross-sectional area of the nanowire, R is the resistance and T is temperature. More details can be found in our previous work.[26,30] With this method, the impact of iridium coating on thermal transport is consequently subtracted and the real thermal diffusivity of pure titania nanowire is obtained and listed in Table I.

IV. CONCLUSION

The TET technology has been used to measure materials featuring different natures and dimensions. Significant nonlinear effects were observed with particular samples, especially the samples that have a small scale and metallic coating. A single anatase TiO_2 nanowire of 340 nm diameter fabricated using the electrospinning technique was used to demonstrate the nonlinear effects. Detailed comparison of rise and fall stages between *U-t* profiles of pure Pt wire and TiO_2 nanowire indicated that the current feed to the nanowire changed with time gradually before it reached a full value. The exact time when the current reached a full value was obscure so that conventional TET data processing was not applicable. Two distinct quantitative methods were developed to suppress these effects. The generalized analysis constrained the nonlinear time-dependent effect into a small term, considering most influences of full current and providing a smooth ratio change with time. The direct derivation method presumed the whole setup to be a simple RC circuit and then directly derived the resistance change against time for the nanowire. The thermal diffusivities determined using both methods agreed well with each other in a range of 2 to 6×10^{-6} m^2/s while a small difference was observed due to the distinct principle differences between these methods. The uncertainty of this fitting was also studied by altering the value of thermal diffusivity to identify significant differences in global data fitting. Compared to the direct derivation method, the generalized analysis is more applicable to situations in which a current source has a relatively long rise time or the material has a relatively fast thermal response.

ACKNOWLEDGMENTS

Support of this work from the National Science Foundation (NSF) (CBET-0931290, CMMI-1029072, CBET-0932573, and CMMI-0926704) is gratefully acknowledged. The authors thank Elizabeth Welch for proofreading the manuscript.

[1]Y. N. Xia, P. D. Yang, Y. G. Sun, Y. Y. Wu, B. Mayers, B. Gates, Y. D. Yin, F. Kim, and Y. Q. Yan, Adv. Mater. **15**(5), 353–389 (2003).
[2]D. G. Cahill, Rev. Sci. Instrum. **61**(2), 802–808 (1990).
[3]D. W. Song, W. L. Liu, T. Zeng, T. Borca-Tasciuc, G. Chen, J. C. Caylor, and T. D. Sands, Appl. Phys. Lett. **77**(23), 3854–3856 (2000).
[4]L. Lu, W. Yi, and D. L. Zhang, Rev. Sci. Instrum. **72**(7), 2996–3003 (2001).
[5]J. B. Hou, X. W. Wang, P. Vellelacheruvu, J. Q. Guo, C. Liu, and H. M. Cheng, J. Appl. Phys. **100**(12), 124314 (2006).
[6]W. J. Parker, R. J. Jenkins, C. P. Butler, and G. L. Abbott J. Appl. Phys. **32**(9), 1679–1684 (1961).
[7]T. Baba and A. Ono, Meas. Sci. Technol. **12**(12), 2046–2057 (2001).
[8]M. Akoshima and T. Baba, Int. J. Thermophys. **26**(1), 151–163 (2005).
[9]M. T. Demko, Z. T. Dai, H. Yan, W. P. King, M. Cakmak, and A. R. Abramson, Rev. Sci. Instrum. **80**(3) (2009).
[10]K. E. Goodson, O. W. Kading, M. Rosler, and R. Zachai, J. Appl. Phys. **77**(4), 1385–1392 (1995).
[11]C. A. Paddock and G. L. Eesley, J. Appl. Phys. **60**(1), 285–290 (1986).
[12]W. S. Capinski, H. J. Maris, T. Ruf, M. Cardona, K. Ploog, and D. S. Katzer, Phys. Rev. B **59**(12), 8105–8113 (1999).
[13]D. C. Chu, M. Touzelbaev, K. E. Goodson, S. Babin, and R. F. Pease, J. Vac. Sci. Technol. B **19**(6), 2874–2877 (2001).
[14]M. J. Assael, S. Botsios, K. Gialou, and I. N. Metaxa, Int. J. Thermophys. **26**(5), 1595–1605 (2005).
[15]T. Borca-Tasciuc, D. A. Borca-Tasciuc, and G. Chen, IEEE Semicond. Ther. 283–291 (2005).
[16]N. Taketoshi, T. Yagi, and T. Baba, Jpn. J. Appl. Phys. **48**(5), 05EC01 (2009).
[17]P. Kim, L. Shi, A. Majumdar, and P. L. McEuen, Phys. Rev. Lett. **87**(21), 215502 (2001).
[18]L. Shi, D. Y. Li, C. H. Yu, W. Y. Jang, D. Kim, Z. Yao, P. Kim, and A. Majumdar, ASME Trans. J. Heat Transfer **125**(5), 881–888 (2003).
[19]D. Y. Li, Y. Y. Wu, P. Kim, L. Shi, P. D. Yang, and A. Majumdar, Appl. Phys. Lett. **83**(14), 2934–2936 (2003).
[20]C. H. Yu, S. Saha, J. H. Zhou, L. Shi, A. M. Cassell, B. A. Cruden, Q. Ngo, and J. Li, ASME Trans. J. Heat Transfer **128**(3), 234–239 (2006).
[21]M. Okuda and S. Ohkubo, Thin Solid Films **213**(2), 176–181 (1992).
[22]B. S. W. Kuo, J. C. M. Li, and A. W. Schmid, Appl. Phys. A **55**(3), 289–296 (1992).
[23]E. T. Ogawa, C. A. Hu, and P. S. Ho, J. Appl. Phys. **86**(11), 6018–6027 (1999).
[24]T. Wang, X. W. Wang, Y. W. Zhang, L. Y. Liu, L. Xu, Y. Liu, L. J. Zhang, Z. Y. Luo, and K. F. Cen, J. Appl. Phys. **104**(1), 013528 (2008).
[25]J. Q. Guo, X. W. Wang, and T. Wang, J. Appl. Phys. **101**(6), 063537 (2007).
[26]X. Feng, X. Wang, X. Chen, and Y. Yue, Acta Mater. **59**(5), 1934–1944 (2011).
[27]X. W. Wang, J. B. Hou, and J. Q. Guo, J. Phys. D: Appl. Phys. **39**(15), 3362–3370 (2006).
[28]T. Wang, X. W. Wang, J. Q. Guo, Z. Y. Luo, and K. Cen, Appl. Phys. A **87**(4), 599–605 (2007).
[29]J. Q. Guo, X. W. Wang, D. B. Geohegan, G. Eres, and C. Vincent, J. Appl. Phys. **103**(11), 113505 (2008).
[30]X. H. Feng and X. W. Wang, Thin Solid Films **519**(16), 5700–5705 (2011).